JOURNAL OF EXPERIMENTAL AND THEORETICAL PHYSICS, 2025, Vol. 167, No. 1, pp. 91–109

ORDER, DISORDER, AND PHASE TRANSITION IN CONDENSED MEDIA

QUANTUM *SU*(3)-FERRIMAGNET ON TRIANGULAR LATTICE IN MAGNETIC FIELD

© 2025 A. S. Martynov, D. M. Dzebisashvili*

Kirensky Institute of Physics, Federal Research Center KSC Siberian Branch, Russian Academy of Science, Krasnoyarsk, Russia

**e-mail: ddm@iph.krasn.ru*

Received July 21, 2024,

Revised August 30, 2024

Accepted September 04, 2024

Abstract. The phase diagrams (magnetic field H – single-ion anisotropy D) for three-sublattice $SU(3)$-ferrimagnet on triangular lattice with mixed sublattice spins ($S = 1,1/2,1/2$) at different values of exchange parameters I (between spins $S = 1$ and $S = 1/2$) and J (between spins $S = 1/2$) are calculated. To correctly account for the algebra of the $SU(3)$ group generators, which includes quadrupole operators, the representation of Hubbard operators was used. It is shown that depending on the system parameters there can be implemented ferrimagnetic Y- or inverted Y ($\bar{Y}$)-phase, canted V-phase (spins $S = 1/2$ are parallel), fan-shaped W-phase, as well as collinear ferrimagnetic and ferromagnetic phases. In the case of $I < J$, a line appears on the phase diagram on which $SU(3)$-ferrimagnet splits into two independent subsystems, one of which is paramagnetic with spins $S = 1$, and the second one is antiferromagnetic with spins $S = 1/2$ in a zero effective magnetic field. In the spin-wave approximation, the dependences of the average values of the quadrupole moment and dipole moments of the three sublattices on the magnetic field and the single-ion anisotropy are calculated. The spin-wave excitation spectrum is analyzed both at $I > J$ and at $I < J$. It is shown that at $I = J$ in the $SU(3)$-ferrimagnet, an accident degeneracy occurs, which can be lifted by taking into account quantum fluctuations.

Keywords: *mixed spin SU(3)-ferrimagnet, single-ion anisotropy, triangular lattice, phase diagrams in magnetic field*.

DOI: 10.31857/S00444510250109e9

1. INTRODUCTION

In recent years, there has been a significant increase in interest in materials where relativistic spin-orbit interaction leads to the manifestation of quantum effects on a macroscopic scale [1, 2]. These materials are commonly referred to as quantum magnets [3]. One of the most striking manifestations of quantum effects is the significant reduction of the average spin value in magnets with $S > 1/2$ [4]. The reason for the spin reduction lies in the consideration of single-ion anisotropy (SIA) arising from spin-orbit interaction or in the inclusion of pairwise interactions associated with higher-order spin invariants of the form $(S_f S_g)^{2S}$ [5–15]. In magnetic systems where such non-Heisenberg interactions are sufficiently strong, spin-nematic phases have been observed. These phases are characterized by zero magnetization even at zero temperature (i.e., complete spin reduction), but they exhibit spontaneous symmetry breaking due to quadrupole order parameters (mean values of operators bilinear in spin components) [10]. The enhancement of such quantum effects is facilitated by frustration [2], low temperature, low system dimensionality [16], and multi-sublattice structures.

For example, in multi-sublattice ferrimagnets with different magnetic ions, the manifestation of quantum effects can be significantly amplified due to the possible compensation of the effective field acting on the spins of magnetically active ions [17–26]. Indeed, as shown in [27], in a two-sublattice ferrimagnet, quantum spin reduction in the anisotropic sublattice (with $S = 1$) at low temperatures can be substantially suppressed by the exchange interaction field from the isotropic sublattice ($S = 1/2$). If there are more than two sublattices, the total effective field from two isotropically antiferromagnetically coupled sublattices acting on the ions of the third anisotropic

sublattice can be nullified, thereby eliminating the mentioned mechanism of spin reduction suppression.

In this regard, one of the key objectives in the theory of quantum magnets is to find a microscopic model that could predict and study new quantum effects with both experimental and practical significance. As outlined above, one promising approach is to investigate the combined action of multiple factors that promote quantum magnetism phenomena. In the context of this research direction, studies such as [28–30] proposed a model of a three-sublattice ferrimagnet with mixed spins $S = 1,1/2,1/2$ on a triangular lattice with Ising exchange interaction and SIA in the $S = 1$ spin subsystem. In those studies, based on Monte Carlo simulations, the main focus was on constructing phase diagrams in the temperature–SIA plane and searching for a technologically significant compensation regime, where the total magnetization reaches zero below the critical temperature. Notably, alongside SIA in the $S = 1$ spin subsystem, the model proposed in [28–30] possessed essential features such as low dimensionality and geometric frustration, which, as mentioned earlier, enhance quantum effects.

In a recent study [31], the authors investigated the SU(3) ferrimagnet (SU3F) model, which closely resembles the model proposed in [28–30] but includes two crucial generalizations. First, instead of Ising exchange interaction, the SU3F model employs isotropic Heisenberg exchange. It is well known that transverse components of exchange interaction in noncollinear magnetic structures induce zero-point quantum fluctuations, leading to antiferromagnetic (AF) fluctuations. These AF fluctuations, like SIA, can cause quantum spin reduction, and therefore, the quantum effects driven by AF and SIA should be distinguished. The second major difference between SU3F and the model proposed in [28–30] lies in the use of different exchange integrals I and J for interactions between the $S = 1$ and $S = 1/2$ sublattices and between the two $S = 1/2$ sublattices, respectively. As shown below, the phase diagrams of SU3F differ qualitatively depending on the ratio between the exchange integrals.

Furthermore, it is essential to highlight an important conceptual feature of the SU3F model. This feature is associated with the fact that significant SIA, as known from previous studies [8–15, 32–36], necessitates the inclusion of the full set of generators of the SU(3) algebra acting in the Hilbert space of the $S = 1$ spin states. Therefore, conventional spin operators are insufficient for describing such systems. To emphasize this aspect, the model proposed in [31] was named the quantum SU(3) ferrimagnet model.

The general characteristic of the SU3F model is the simultaneous consideration of several factors that enhance quantum effects: SIA, AF fluctuations, multi-sublattice structure, low dimensionality, and exchange frustration.

The study of the SU3F model in [31] was conducted in the absence of an external magnetic field and at zero temperature. The dependence of the sublattice spin moments and the quadrupole moment on the SIA parameter was calculated for different exchange integral ratios I/J. It was found that the critical value of the SIA parameter D_c, at which SU3F transitions to the quadrupole phase, can be significantly smaller than both I and J. Moreover, for $I > J$, a compensation point was observed in the total moment M dependence on the SIA parameter, i.e., M at $D < D_c$.

This work represents a logical continuation of the studies conducted in [31]. Its primary goal is to construct the phase diagram of SU3F in the external magnetic field–SIA parameter plane and to analyze the modification of the magnetic structure and order parameters when crossing the phase boundaries. The ground state energy and the corresponding spin configuration are calculated within the mean-field approximation at zero temperature. This condition, as is well known, is unachievable by the Monte Carlo method used in the previously cited works [28–30]. To correctly account for the SU(3) algebra generators in the $S = 1$ spin subsystem, the Hubbard operator formalism is employed [11, 35, 37]. In the calculation of order parameters, spin operator bosonization is applied: the Holstein–Primakoff transformation for the $S = 1/2$ spin subsystem and the indefinite metric formalism for the $S = 1$ subsystem [11, 14].

The remainder of this paper is organized as follows. Section 2 formulates the SU3F Hamiltonian in an external magnetic field lying in the easy-plane direction. Section 3 presents the $SU(2)$ transformation of the S = 1/2S = 1/2S = 1/2 spin operators, corresponding to the rotation of local coordinate axes. Section 4 details the Holstein–Primakoff transformation for the $S = 1/2$ spin subsystem. Section 5 describes the transition to the Hubbard operator representation and their triple

$SU(3)$ transformation for diagonalizing the single-ion Hamiltonian of the $S = 1$ spin subsystem. The bosonization of Hubbard operators and the derivation of the dispersion equation are covered in Section 6. Sections 7 and 8 analyze the characteristics of phase diagrams and the changes in order parameters for $I < J$ and $I > J$, respectively. Section 9 demonstrates the degeneracy of the SU3F mean-field ground state at $I = J$. Section 10 discusses changes in the spin-wave excitation spectrum as the magnetic field increases under different exchange parameter ratios. The main conclusions of the study are presented in Section 11.

2. MODEL OF $SU3$-FERRIMAGNETISM

The crystal structure of the considered SU3F is shown in Fig. 1. The red circles mark the lattice sites of the sublattice with spin value $S = 1$, further referred to as the L-sublattice. The green and blue circles mark the lattice sites of the sublattices with spin value $S = 1/2$, denoted further as F and G sublattices, respectively. The periodicity of the system is defined by the basis vectors a_1 and a_2, equal in magnitude. The vectors z and x connect the nodes of different sublattices.

The Hamiltonian of SU3F in an external magnetic field can be written as:

$$\mathcal{H} = \mathcal{H}_A + \mathcal{H}_{exch} + \mathcal{H}_{field}, \qquad (1)$$

where:

$$\mathcal{H}_{exch} = J\sum_{\{fg\}} S_f S_g + I\sum_{\{fl\}} S_f S_l + I\sum_{\{gl\}} S_g S_l,$$

$$\mathcal{H}_A = D\sum_l \left(S_l^y\right)^2, \qquad (2)$$

$$\mathcal{H}_{field} = -h\sum_f S_f^z - h\sum_g S_g^z - h_L\sum_l S_l^z.$$

The operator $\mathcal{H}_{exch}$ describes the pairwise exchange interaction between the nearest-neighbor spins from different sublattices. The lower indices f, g and l of the spin operators denote the lattice sites from the F-, G- and L sublattices, respectively. The exchange integral J determines the strength of the antiferromagnetic interaction between the nearest-neighbor spins from the F- and G- sublattices, while the integral I governs the interaction between the $F(G)$- and L- sublattices. The curly brackets under the summation symbols in (2) indicate that the summation is carried out only over nearest neighbors, with each pair of nodes counted only once.

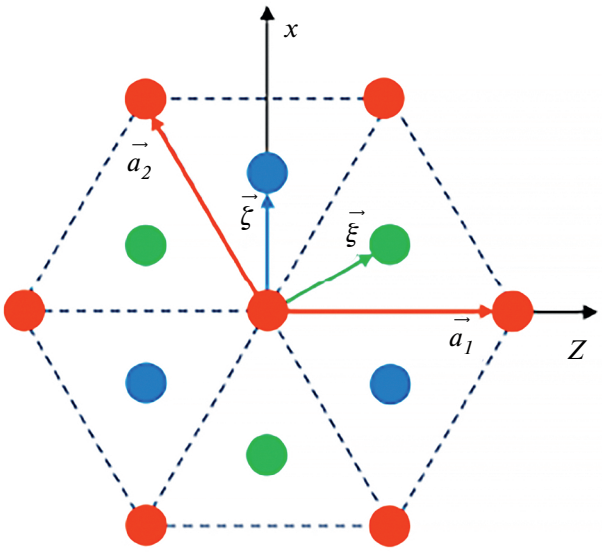

Fig. 1. Crystal structure of the three-sublattice SU3F on a triangular lattice. Red, green, and blue circles indicate the positions of the nodes in the L-, F- and G- sublattices, respectively. $|a_1| = |a_2| = a$ are the Bravais lattice vectors, while ξ and ζ represent the basis vectors.

The operator $\mathcal{H}_A$ describes the effect of single-ion anisotropy (SIA) of the easy-plane type acting on the spins $S = 1$ in the L- sublattice. The anisotropy parameter D is positive. The y axis is directed perpendicular to the ferrimagnet plane xz, which is, therefore, the easy magnetization plane.

The operator $\mathcal{H}_{field}$ accounts for the Zeeman energy of the spins in the external magnetic field H, lying in the ferrimagnet plane (easy plane) and determining the parameters $h = g\propto_B H$, and $h_L = g_L\propto_B H$, where $\propto_B$ is the Bohr magneton, and g and g_L are the Landé factors for the $F(G)$-sublattices, respectively. In general, the g-factors may differ for different sublattices. In this study, we assume that the moments are formed without the participation of orbital degrees of freedom, i.e., they are purely spin-related, so $g_L = g = 2$.

The direction of the magnetic field and the type of SIA ensure that the average moment of the L sublattice of R_L, is oriented in the xz plane, perpendicular to the anisotropy axis y. Furthermore, considering the nature of the exchange interactions and the results of Ref. [38], it can be argued that the magnetic structure of the SU3F ground state for any values of D and H is characterized by a planar

configuration of spin expectation values. Therefore, without loss of generality, we will assume that the spins of all three sublattices lie in the ferrimagnet plane xz, with the z axis of the original coordinate system conveniently directed along the magnetic field.

3. $SU(3)$-TRANSFORMATION OF THE HAMILTONIAN

To calculate the ground-state energy of SU3F, it is convenient to start with a unitary transformation of the Hamiltonian H:

$$\mathcal{H}(\theta_F,\theta_G) = U_2(\theta_F,\theta_G)\mathcal{H}U_2^{+}(\theta_F,\theta_G), \qquad (3)$$

with the operator

$$U_2(\theta) = \prod_{f\in F}\exp\left(-i\theta_F S_f^y\right)\prod_{g\in G}\exp\left(-i\theta_G S_g^y\right). \qquad (4)$$

The transformation (3) allows one to switch to new local coordinates for the F - and G - sublattices, where the quantization axes z' and z'' are rotated by the angles θ_F and θ_G around the y axis, aligning them along the equilibrium magnetizations R_F and R_G, respectively (see Fig. 2).

The unitary transformation (3) of the Hamiltonian (1) corresponds to the following formal substitution of the spin operators for the F- and G- sublattices [39]:

$$S_f^x \to S_f^x\cos\theta_F + S_f^z\sin\theta_F,\ S_f^y \to S_f^y,$$
$$S_f^z \to S_f^z\cos\theta_F - S_f^x\sin\theta_F, \qquad (5)$$
$$S_g^x \to S_g^x\cos\theta_G + S_g^z\sin\theta_G,\ S_g^y \to S_g^y,$$
$$S_g^z \to S_g^z\cos\theta_G - S_g^x\sin\theta_G. \qquad (6)$$

As a result, the Hamiltonian operator (1) is transformed into the following form:

$$\mathcal{H} = D\sum_l (S_l^y)^2 +$$
$$+J\sum_{\{fg\}}\left\{(S_f^xS_g^x + S_f^zS_g^z)\cos(\theta_F-\theta_G) + \right.$$
$$\left.+S_f^yS_g^y + (S_f^zS_g^x - S_f^xS_g^z)\sin(\theta_F-\theta_G)\right\} +$$
$$+I\sum_{\{fl\}}\left\{(S_f^xS_l^x + S_f^zS_l^z)\cos\theta_F + S_f^yS_l^y + \right.$$
$$\left.+(S_f^zS_l^x - S_f^xS_l^z)\sin\theta_F\right\} +$$

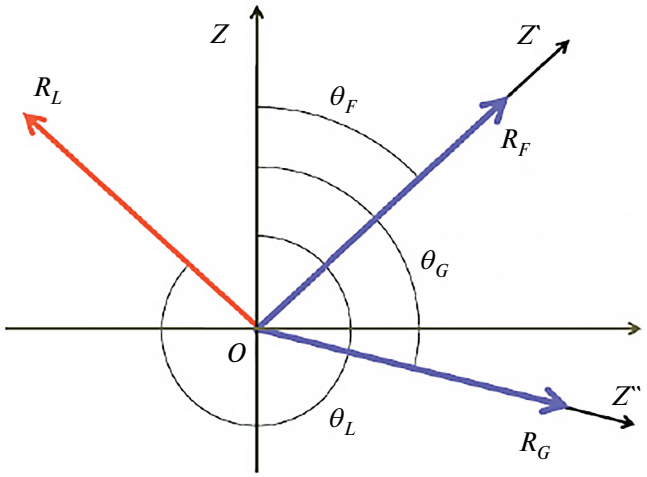

Fig. 2. Rotation of local coordinate axes during the unitary transformation (3). In the F- and G- sublattices with $S = 1/2$, the axes z are rotated by the angles θ_F and θ_G, taking new positions z' and z'', respectively. The local coordinates in the L- subsystem with $S = 1$ remain unchanged, while the angle formed by the moment $R_L$and the z axis is denoted by θ_L.

$$+I\sum_{\{gl\}}\left\{(S_g^xS_l^x + S_g^zS_l^z)\cos\theta_G + S_g^yS_l^y + \right.$$
$$\left.+(S_g^zS_l^x - S_g^xS_l^z)\sin\theta_G\right\} -$$
$$-h\sum_f\left\{S_f^z\cos\theta_F - S_f^x\sin\theta_F\right\} -$$
$$-h\sum_g\left\{S_g^z\cos\theta_G - S_g^x\sin\theta_G\right\} - h_L\sum_l S_l^z, \qquad (7)$$

where the operators S_f^β and S_g^β ($\beta = x,y,z$) relating to F- and G-subsystems refer to the projections of the spin moments on the quantization axes corresponding to index β in the new (rotated) local coordinate systems.

4. HOLSTEIN–PRIMAKOFF TRANSFORMATION

Following the strategy outlined in the introduction for calculating the ground-state energy of SU3F, we perform the Holstein–Primakoff transformation separately for the F- and G- sublattices:

$$S_f^+ = \sqrt{2S - a_f^+a_f}\cdot a_f,\quad S_f^z = S - a_f^+a_f,$$
$$S_g^+ = \sqrt{2S - b_g^+b_g}\cdot b_g,\quad S_f^z = S - b_g^+b_g, \qquad (8)$$

where the bosonic creation $a_f^+(b_g^+)$ and annihilation $a_f(b_g)$ operators describe spin transitions at site $f(g)$ of the $F(G)$ sublattice from the state $|\uparrow'\rangle(|\uparrow''\rangle)$, corresponding to spin orientation along the $z'(z'')$

axis, to the opposite orientation $|\downarrow'\rangle(|\downarrow''\rangle)$, and vice versa.

Substituting (8) into the Hamiltonian (7) gives the result:

$$\mathcal{H} = E_0 + \mathcal{H}^{(0)} + \mathcal{H}^{(1)} + \mathcal{H}^{(2)}. \tag{9}$$

where:

$$E_0 = J_0 S^2 N \cos(\theta_F - \theta_G) - \\ -hSN(\cos\theta_F + \cos\theta_G), \tag{10}$$

Here, $H^{(n)}$ $(n = 0,1,2)$ denotes the number of sites in the sublattice. The Hamiltonian $H^{(0)}$ represents the sum of the single-ion Hamiltonians for the L- subsystem:

$$\mathcal{H}^{(0)} = \sum_l \mathcal{H}_0(l),$$

where:

$$\mathcal{H}_0(l) = D(S_l^y)^2 + \bar{H}_z S_l^z + \bar{H}_x S_l^x, \tag{11}$$

The effective fields are defined as:

$$\bar{H}_z = I_0 S(\cos\theta_F + \cos\theta_G) - h_L, \\ \bar{H}_x = I_0 S(\sin\theta_F + \sin\theta_G), \; I_0 = 3I. \tag{12}$$

The linear term in bosonic operators from the Hamiltonian (9) can be written as:

$$\mathcal{H}^{(1)} = \sum_{\{fl\}} I\sqrt{\frac{S}{2}}\left[\cos\theta_F S_l^x - \sin\theta_F S_l^z\right](a_f + a_f^+) + \\ + \sum_f \sqrt{\frac{S}{2}}\left[J_0 S\sin(\theta_G - \theta_F) + h\sin\theta_F\right](a_f + a_f^+) + \\ + \sum_{\{gl\}} I\sqrt{\frac{S}{2}}\left[\cos\theta_G S_l^x - \sin\theta_G S_l^z\right](b_g + b_g^+) + \\ + \sum_g \sqrt{\frac{S}{2}}\left[J_0 S\sin(\theta_F - \theta_G) + h\sin\theta_G\right](b_g + b_g^+) + \\ + \frac{I}{i}\sqrt{\frac{S}{2}}\left\{\sum_{\{fl\}} S_l^y (a_f - a_f^+) + \sum_{\{gl\}} S_l^y (b_g - b_g^+)\right\}, \tag{13}$$

where:

$$J_0 = 3J$$

The last term in expression (9) describes the excitations in the F- and G subsystems and has the form:

$$\mathcal{H}^{(2)} = J\frac{S}{2}\sum_{\{f,g\}}\left\{\left[(a_f + a_f^+)(b_g + b_g^+) - \right.\right. \\ \left. - 2(a_f^+ a_f + b_g^+ b_g)\right]\cos(\theta_F - \theta_G) - \\ - (a_f - a_f^+)(b_g - b_g^+)\Big\} - \\ - I\sum_{\{f,l\}}(\cos\theta_F S_l^z + \sin\theta_F S_l^x)a_f^+ a_f - \\ - I\sum_{\{g,l\}}(\cos\theta_G S_l^z + \sin\theta_G S_l^x)b_g^+ b_g + \\ + h\cos\theta_F\sum_f a_f^+ a_f + h\cos\theta_G\sum_g b_g^+ b_g. \tag{14}$$

Next, the mean-field logic dictates replacing the spin operators $H^{(1)}$ and $H^{(2)}$ of the L- subsystems with their average values. In the considered zero-temperature regime, averaging the operators S_l^α $(\alpha = x,y,z)$ is sufficient to perform based on the ground state of the single-site Hamiltonian (11).

5. DIAGONALIZATION OF THE SINGLE-ION HAMILTONIAN

To diagonalize the single-ion Hamiltonian (11), we use the approach developed in [40]. We transition from spin operators to Hubbard operators [37], where $X_l^{m,n} = |m\rangle\langle n|$, where $m,n = \{-1,0,+1\}$ are the eigenstates of the operator S_l^z with corresponding eigenvalues $|m\rangle$ and $|n\rangle$ of $S_l^z|n\rangle = n|n\rangle$. Substituting

$$S_l^x = \frac{1}{\sqrt{2}}\left(X_l^{1,0} + X_l^{\bar{1},0} + X_l^{0,1} + X_l^{0,\bar{1}}\right), \\ S_l^y = \frac{i}{\sqrt{2}}\left(-X_l^{1,0} + X_l^{\bar{1},0} + X_l^{0,1} - X_l^{0,\bar{1}}\right), \\ (S_l^y)^2 = \frac{1}{2}\left(X_l^{1,\bar{1}} + X_l^{\bar{1},1} - X_l^{1,1} - X_l^{\bar{1},\bar{1}}\right) + X_l^{0,0}, \\ S_l^z = X_l^{1,1} - X_l^{\bar{1},\bar{1}}, \quad \bar{1} \equiv -1, \tag{15}$$

Describing the transition to representation of the Hubbard operators into the single-ion Hamiltonian (11) gives:

$$\mathcal{H}_0(l) = \left(\frac{D}{2} + \bar{H}_z\right)X_l^{1,1} + DX_l^{0,0} + \\ + \left(\frac{D}{2} - \bar{H}_z\right)X_l^{\bar{1},\bar{1}} - \frac{D}{2}\left(X_l^{1,\bar{1}} + X_l^{\bar{1},1}\right) + \\ + \frac{\bar{H}_x}{\sqrt{2}}\left(X_l^{1,0} + X_l^{0,1} + X_l^{\bar{1},0} + X_l^{0,\bar{1}}\right). \tag{16}$$

In the absence of a magnetic field, the ground state of the system is degenerate with respect to rotations around the y axis. Choosing the x axis

along the vector R_L and assuming equivalence between the F - and G -sublattices ($\theta_F = -\theta_G$,), the parameter φ\phiφ becomes zero, and the last term in (16) vanishes. In this case, the Hamiltonian $H_0(l)$ couples only two of the three states ($|+1\rangle$ and $|-1\rangle$), and its diagonalization requires only one unitary transformation (see [31]). However, the presence of a magnetic field couples all three states $|n\rangle$ ($n = \{-1,0,+1\}$), requiring three consecutive transformations for the diagonalization of the single-ion Hamiltonian.

The unitary operator $U_{nm}(\alpha,l)$ for each transformation is defined by its generator $\Gamma_{nm}(l) = X_l^{nm} - X_l^{mn}$ from the SU(3) group, according to the expression:

$$U_{nm}(\alpha,l) = \exp\{\alpha\Gamma_{nm}(l)\} =$$
$$= 1 + (\cos\alpha - 1)(X_l^{nm} + X_l^{mn}) + \sin\alpha\,\Gamma_{nm}(l). \quad (17)$$

The new Hubbard operators $X_l^{\tilde{r}\tilde{s}} = |\tilde{r},l\rangle\langle\tilde{s},l|$, defined through the new basis states

$$|\tilde{r},l\rangle = U_{nm}(-\alpha,l)|r,l\rangle, \quad (18)$$

are expressed via original Hubbard operators as follows:

$$X_l^{\tilde{r}\tilde{s}} = U_{nm}(-\alpha,l)\,X_l^{rs}\,U_{nm}^{+}(-\alpha,l). \quad (19)$$

Thus, the unitary transformation reduces to a simple substitution in the single-site Hamiltonian:

$$X_l^{rs} \to U_{\tilde{n}\tilde{m}}(\alpha,l)\,X_l^{\tilde{r}\tilde{s}}\,U_{\tilde{n}\tilde{m}}^{+}(\alpha,l). \quad (20)$$

Explicit expressions for the right-hand side of the last formula were derived in [40] and are provided in Appendix A for completeness. The variational parameter α in (17) is chosen such that the off-diagonal terms $X_l^{\tilde{n}\tilde{m}}$ and $X_l^{\tilde{m}\tilde{n}}$ vanish in the transformed Hamiltonian.

Performing the three consecutive unitary transformations with the operators $U_{1,0}(\alpha_2)$, $U_{0,-1}(\alpha_3)$ and $U_{1,-1}(\alpha_1)$, following the rule (20), and retaining the original notation for the indices of the new states $n = \{-1,0,+1\}$ (i.e., without tildes), we obtain the diagonal form of the single-ion Hamiltonian $H_0(l)$:

$$\mathcal{H}_0(l) = \sum_n \varepsilon_n X_l^{nn}, \quad n = -1,0,+1. \quad (21)$$

The eigenvalues ε_n of the single-ion Hamiltonian can be expressed as ($\bar{1} = -1$):

$$\varepsilon_1 = e_{\bar{1},\bar{1}}\sin^2\alpha_1 + e_{1,1}\cos^2\alpha_1 + e_{1,\bar{1}}\sin 2\alpha_1,$$
$$\varepsilon_{\bar{1}} = e_{\bar{1},\bar{1}}\cos^2\alpha_1 + e_{1,1}\sin^2\alpha_1 - e_{1,\bar{1}}\sin 2\alpha_1, \quad (22)$$
$$\varepsilon_0 = e_{0,0},$$

where

$$e_{1,1} = D\sin^2\alpha_2 + \left(\frac{D}{2} + \bar{H}_z\right)\cos^2\alpha_2 +$$
$$+\frac{\bar{H}_x}{\sqrt{2}}\sin 2\alpha_2,$$
$$e_{\bar{1},\bar{1}} = D\cos^2\alpha_2\sin^2\alpha_3 - \frac{D}{2}\sin\alpha_2\sin 2\alpha_3 +$$
$$+\left(\frac{D}{2} + \bar{H}_z\right)\sin^2\alpha_2\sin^2\alpha_3 +$$
$$+\left(\frac{D}{2} - \bar{H}_z\right)\cos^2\alpha_3 - \quad (23)$$
$$-\frac{\bar{H}_x}{\sqrt{2}}(\cos\alpha_2\sin 2\alpha_3 + \sin 2\alpha_2\sin^2\alpha_3),$$
$$e_{0,0} = D\cos^2\alpha_2\cos^2\alpha_3 + \frac{D}{2}\sin\alpha_2\sin 2\alpha_3 +$$
$$+\left(\frac{D}{2}+\bar{H}_z\right)\sin^2\alpha_2\cos^2\alpha_3+\left(\frac{D}{2}-\bar{H}_z\right)\sin^2\alpha_3 +$$
$$+\frac{\bar{H}_x}{\sqrt{2}}(\cos\alpha_2\sin 2\alpha_3 - \sin 2\alpha_2\cos^2\alpha_3),$$

$$e_{1,\bar{1}} = \left(\frac{\bar{H}_z}{2} - \frac{D}{4}\right)\sin(2\alpha_2)\sin\alpha_3 -$$
$$-\frac{D}{2}\cos\alpha_2\cos\alpha_3 +$$
$$+\frac{\bar{H}_x}{\sqrt{2}}(-\cos 2\alpha_2\sin\alpha_3 + \sin\alpha_2\cos\alpha_3).$$

From the requirement of nullifying the coefficients of the non-diagonal X-operators in the transformed Hamiltonian, the following system of equations for the angles α_j ($j = 1,2,3$) is obtained:

$$\mathrm{tg}\alpha_3 = \frac{\left(\frac{D}{2} - \bar{H}_z\right)\sin 2\alpha_2 + \sqrt{2}\,\bar{H}_x\cos 2\alpha_2}{D\cos\alpha_2 - \sqrt{2}\,\bar{H}_x\sin\alpha_2},$$
$$\mathrm{tg}2\alpha_3 = \frac{\sqrt{2}\,\bar{H}_x\cos\alpha_2 + D\sin\alpha_2}{2\bar{H}_z + \left(\frac{D}{2} - \bar{H}_z\right)\cos^2\alpha_2 - \frac{\bar{H}_x}{\sqrt{2}}\sin 2\alpha_2}, \quad (24)$$
$$2\alpha_1 = 2e_{1,\bar{1}} / (e_{1,1} - e_{\bar{1},\bar{1}}).$$

Similarly, by sequentially applying formula (20) with the operators $U_{1,0}(\alpha_2)$, $U_{0,\bar{1}}(\alpha_3)$ and $U_{1,\bar{1}}(\alpha_1)$, to the representation (15), the spin operators S_l^x, S_l^y, S_l^z and $(S_l^y)^2$ can be expressed through the new (transformed) X-operators. The expansion coefficients of the spin operators S_l^α in terms of the new Hubbard operators X_l^{nm} will represent the matrix elements of the spin operators in the new states: $s_{n,m}^\alpha \equiv \langle n \mid S_l^\alpha \mid m \rangle$ ($\alpha = x,y,z$). Explicit expressions for these matrix elements are given in Appendix B.

Within the mean-field approximation, the spin operators in the Hamiltonian $H^{(1)}$ should be replaced by their average values, i.e., the diagonal matrix elements $s_{n,n}^\alpha$, calculated for the ground state $|n\rangle$, corresponding to the minimum value of ε_n. Below, we will choose the set of solutions of equations (24) for the angles α_j ($j = 1,2,3$) such that the state $|+1\rangle$ is the ground state.

Since $s_{nn}^y = 0$ for any n (see Appendix B), the last two sums in formula (13) for $H^{(1)}$ vanish. The reduction of the remaining terms in (13) occurs under the conditions:

$$\begin{aligned} &I_0(s_{1,1}^x \cos\theta_F - s_{1,1}^z \sin\theta_F) + \\ &+ J_0 S \sin(\theta_G - \theta_F) + h \sin\theta_F = 0, \\ &I_0(s_{1,1}^x \cos\theta_G - s_{1,1}^z \sin\theta_G) + \\ &+ J_0 S \sin(\theta_F - \theta_G) + h \sin\theta_G = 0, \end{aligned} \tag{25}$$

These conditions will be further used to determine the equilibrium values of the angles θ_F and θ_G. The angle θ_L, introduced in Fig. 2 for clarity, is not a tuning parameter and can be determined through the ratio of the average values of the spin projections S_l^z and S_l^x.

The magnetic structure of the SU3F ground state is determined by the solutions of the five equations (24) and (25) for the angles α_j ($j = 1,2,3$), θ_F and θ_G, followed by the selection of the solution set that corresponds to the minimum value of the mean-field energy of the entire system:

$$E_{MF} = E_0 + N\varepsilon_1, \tag{26}$$

where the values E_0 and ε_1 are defined by equations (10) and (22), respectively. In Section 7, the SU3F phase diagrams in the $h - D$ -coordinates, calculated based on the methodology presented here, will be presented.

6. BOSONIZATION OF THE L- SUBSYSTEM AND THE DISPERSION EQUATION

Within the chosen approximation, the ground state energy E_{MF} is determined without considering AF (antiferromagnetic) contributions. Therefore, the contributions from the last term in the Hamiltonian (9), quadratic in Bose operators, are absent in expression (26) for E_{MF}. Nevertheless, when calculating the dependencies of order parameters on the magnetic field and single-ion anisotropy (SIA), the energy spectrum of spin-wave excitations is required, and to determine this spectrum, the operator $H^{(2)}$ must be taken into account.

To compute the energy spectrum within the spin-wave approximation, we first express the spin operators through the new (transformed) X-operators. Using (15) and the formulas from Appendix A, we obtain expressions for the S-operators of the form:

$$S_l^\alpha = \sum_{n,m} s_{nm}^\alpha X_l^{nm}, \quad \alpha = x,y,z, \tag{27}$$

where the matrix elements s_{nm}^α are given in Appendix B.

Next, considering that the state spectrum $H_0(l)$ is characterized by three levels and the ground state of the single-ion Hamiltonian is the state $|+1\rangle$, we introduce, following [11, 14], two types of Bose operators: c and d. The creation of one $c(d)$ boson at site l is described by the creation operator $c_l^+(d_l^+)$ and corresponds to the system transitioning from the "vacuum" state $|+1\rangle$ to the state $|0\rangle(|-1\rangle)$ with one $c(d)$ boson. The Hermitian conjugate operator $c_l(d_l)$, acting in the opposite direction, annihilates the $c(d)$ boson. States with more than one boson are excluded by the metric operator as non-physical.

The representation of Hubbard operators through Bose operators, proposed in [40] within the framework of the indefinite metric formalism [41], takes the form:

$$\begin{aligned} &X_l^{1,0} = (1 - c_l^+ c_l - d_l^+ d_l) c_l,\ X_l^{0,1} = c_l^+, \\ &X_l^{1,\bar{1}} = (1 - c_l^+ c_l - d_l^+ d_l) d_l,\ X_l^{\bar{1},1} = d_l^+, \\ &X_l^{0,\bar{1}} = c_l^+ d_l,\ \ X_l^{\bar{1},0} = d_l^+ c_l,\ \ X_l^{0,0} = c_l^+ c_l, \\ &X_l^{\bar{1},\bar{1}} = d_l^+ d_l,\ \ X_l^{1,1} = (1 - c_l^+ c_l - d_l^+ d_l). \end{aligned} \tag{28}$$

We use the representation (28) in the formulas (27) and substitute the resulting expressions for the S-operators (see Appendix C) into the terms $H^{(1)}$

and $H^{(2)}$ of the Hamiltonian (9). As a result, an expression arises in which only contributions up to the second order in the a, b, c and d - operators should be retained. Performing the Fourier transform:

$$a_f = \frac{1}{\sqrt{N}}\sum_k e^{ikf} a_k, \quad b_g = \frac{1}{\sqrt{N}}\sum_k e^{ikg} b_k,$$
$$c_l = \frac{1}{\sqrt{N}}\sum_k e^{ikl} c_k, \quad d_l = \frac{1}{\sqrt{N}}\sum_k e^{ikl} d_k, \tag{29}$$

we obtain the desired Hamiltonian, which can be written as follows:

$$H = E_{MF} + H_{SW}. \tag{30}$$

Here, the first term E_{MF} corresponds to the ground state energy in the mean-field approximation (see formula (26)), while the second term H_{SW} describes spin-wave excitations and is defined by the expression:

$$\begin{aligned} H_{SW} = \sum_k \{ & E_a a_k^+ a_k + E_b b_k^+ b_k + E_c c_k^+ c_k + E_d d_k^+ d_k + \\ & + J_+(\gamma_k a_k^+ b_k + \gamma_k^* b_k^+ a_k)\} + \\ & + J_-(\gamma_k a_k^+ b_{-k}^+ + \gamma_k^* a_k b_{-k}) + \\ & + I_{0F}^+(\gamma_k c_k^+ a_k + \gamma_k^* a_k^+ c_k) + \\ & + I_{0F}^-(\gamma_k c_k^+ a_{-k}^+ + \gamma_k^* c_k a_{-k}) + \\ & + I_{\bar{1}F}^+(\gamma_k d_k^+ a_k + \gamma_k^* a_k^+ d_k) + \\ & + I_{\bar{1}F}^-(\gamma_k d_k^+ a_{-k}^+ + \gamma_k^* d_k a_{-k}) + \\ & + I_{0G}^+(\gamma_k^* c_k^+ b_k + \gamma_k b_k^+ c_k) + \\ & + I_{0G}^-(\gamma_k^* c_k^+ b_{-k}^+ + \gamma_k c_k b_{-k}) + \\ & + I_{\bar{1}G}^+(\gamma_k^* d_k^+ b_k + \gamma_k b_k^+ d_k) + \\ & + I_{\bar{1}G}^-(\gamma_k^* d_k^+ b_{-k}^+ + \gamma_k d_k b_{-k}). \end{aligned} \tag{31}$$

In this expression, the following notations were introduced:

$$\begin{aligned} E_a &= -J_0 S\cos(\theta_F - \theta_G) + h\cos\theta_F - \\ &\quad - I_0(s_{11}^z\cos\theta_F + s_{11}^x\sin\theta_F), \\ E_b &= -J_0 S\cos(\theta_G - \theta_F) + h\cos\theta_G - \\ &\quad - I_0(s_{11}^z\cos\theta_G + s_{11}^x\sin\theta_G), \end{aligned}$$

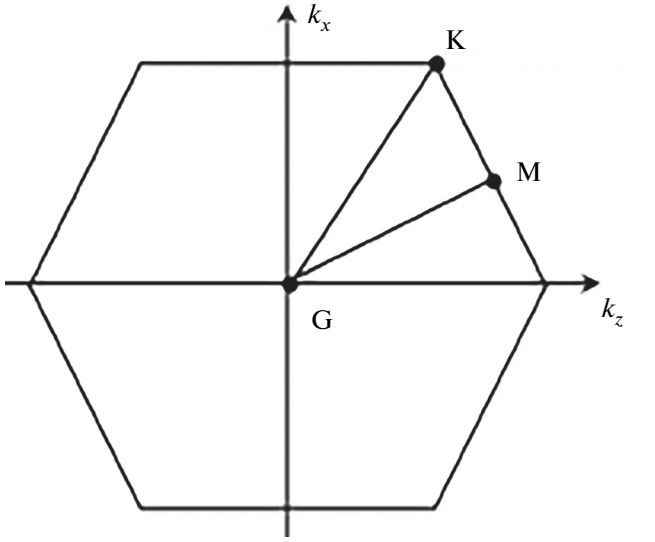

Fig. 3. The Brillouin zone of the triangular lattice and three high-symmetry points: Γ, *K*, *M*.

$$\begin{aligned} E_c &= \varepsilon_0 - \varepsilon_1, \quad E_d = \varepsilon_{\bar{1}} - \varepsilon_1, \\ J_\pm &= \frac{J_0 S}{2}(\cos(\theta_F - \theta_G) \pm 1), \\ I_{nA}^\pm &= I_0\sqrt{\frac{S}{2}}\left(s_{n1}^x\cos\theta_A - s_{n1}^z\sin\theta_A \pm \frac{s_{n1}^y}{i}\right), \\ n &= \{0,\bar{1}\}, \quad A = \{F,G\}, \\ \gamma_k &= \frac{1}{3}\sum_\delta e^{ik\delta} = \frac{1}{3}\left(2\cos\frac{k_z}{2}e^{i\frac{k_x}{2\sqrt{3}}} + e^{-i\frac{k_x}{\sqrt{3}}}\right). \end{aligned} \tag{32}$$

In the sum defining the triangular lattice invariant γ_k, the vector δ takes three values: $\{\xi, -\zeta, \zeta - \xi\}$ (see Fig. 1). The Brillouin zone, which bounds the region of quasimomentum values, is shown in Fig. 3.

To obtain the dispersion equation, we define the matrix retarded Green's function $\langle\langle X_k \mid X_k^+\rangle\rangle_\omega$,, where

$$X_k^+ = (a_k^+, b_k^+, c_k^+, d_k^+, a_{-k}, b_{-k}, c_{-k}, d_{-k}).$$

From the requirement for nontrivial solutions of the equation of motion for $\langle\langle X_k \mid X_k^+\rangle\rangle_\omega$, the spectrum equation follows:

$$\begin{vmatrix} \omega - A_k & -B_k \\ B_k & \omega + A_k \end{vmatrix} = 0, \tag{33}$$

where

$$A_k = \begin{pmatrix} E_a & J_+\gamma_k & I^+_{0F}\gamma^*_k & I^+_{\bar{1}F}\gamma^*_k \\ J_+\gamma^*_k & E_b & I^+_{0G}\gamma_k & I^+_{\bar{1}G}\gamma_k \\ I^+_{0F}\gamma_k & I^+_{0G}\gamma^*_k & E_c & 0 \\ I^+_{\bar{1}F}\gamma_k & I^+_{\bar{1}G}\gamma^*_k & 0 & E_d \end{pmatrix} \quad (34)$$

and

$$B_k = \begin{pmatrix} 0 & J_-\gamma_k & I^-_{0F}\gamma^*_k & I^-_{\bar{1}F}\gamma^*_k \\ J_-\gamma^*_k & 0 & I^-_{0G}\gamma_k & I^-_{\bar{1}G}\gamma_k \\ I^-_{0F}\gamma_k & I^-_{0G}\gamma^*_k & 0 & 0 \\ I^-_{\bar{1}F}\gamma_k & I^-_{\bar{1}G}\gamma^*_k & 0 & 0 \end{pmatrix}. \quad (35)$$

7. SU3F PHASE DIAGRAM FOR $I < J$

We will discuss the SU3F phase diagram in the magnetic field–anisotropy parameter (D) coordinates separately for three cases of exchange parameter ratios: $I < J$, $I > J$, $I = J$. In this section, we consider the first case: $I < J$.

Fig. 4 shows the phase diagram of the SU3F ground state, calculated according to the methodology outlined in Section 5, for the exchange parameter ratio $I / J = 0.8$. It is evident that three phases are realized in the considered regime: the inverted Y-phase (hereinafter referred to as $\bar{Y}$), the W-phase, and the ferromagnetic phase.

In the $\bar{Y}$ phase, the average spin vector of the L-sublattice, R_L is aligned along the magnetic field direction (the z-axis), while the average spin vectors of the F- and G- sublattices, R_F and R_G, form equal but opposite angles with the z-axis: $\theta_F = -\theta_G$. The magnitude of the angles θ_F and θ_G varies within the range $[\pi/2, \pi]$.

In the symmetric W-phase, the angles θ_F and θ_G also have equal magnitudes and opposite signs. However, unlike the $\bar{Y}$ phase, the range of these angle magnitudes is different: $[0,\pi/2]$. In this case, the projections of all three vectors R_F, R_G and R_L onto the z-axis are positive. The boundary between the $\bar{Y}$- and W-phases in Fig. 4 is marked by the dashed line. To the right of the red line on the phase diagram, the ferromagnetic phase is realized: the average spin vectors of the L-, F- and G- sublattices are aligned along the magnetic field.

The evolution of the magnetic structure as the magnetic field at $I < J$ is characterized by a monotonic decrease in the absolute values of

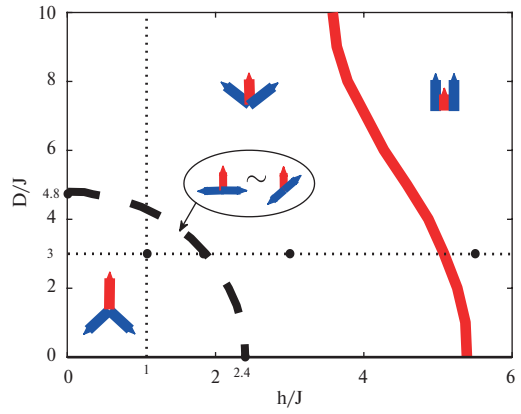

Fig. 4. The h–D phase diagram of the SU3F ground state for $I/J = 0.8$. The black dashed line corresponds to the boundary between the $\bar{Y}$- and W-phases, while the solid red line indicates the boundary between the W phase and the ferromagnetic phase. The pictograms illustrating the magnetic structure of SU3F represent the R_L vector with a red arrow, the $R_{F(G)}$, vectors with blue arrows, and the magnetic field h directed upward. On the dashed line, a phase is realized where the subsystems with spins S = 1 and 1/2 become effectively independent.

the angles θ_F and θ_G, as H increases which vanish at a certain field value dependent on the anisotropy parameter OA (see the red line in Fig. 4). This behavior is illustrated by three pictograms schematically depicting the magnetic structure in each of the three regions of the phase diagram.

To further understand the presented phase diagram, we will calculate the dependence of the SU3F order parameters on the magnetic field for a fixed anisotropy parameter OA and on the anisotropy parameter OA for a fixed magnetic field h.

The average spin values R_F and R_G in F- and G-sublattices can be calculated using the Holstein–Primakoff representation (8), according to which:

$$\begin{aligned} R_F &= \langle S^{z'}_f \rangle = S - n_a, \\ R_G &= \langle S^{z''}_g \rangle = S - n_b, \end{aligned} \quad (36)$$

where the boson occupation numbers $n_a = \langle a^+_f a_f \rangle$ and $n_b = \langle b^+_g b_g \rangle$ are computed using the spectral theorem from the matrix Green's function $\langle\langle X_k \mid X^+_k \rangle\rangle_\omega$ introduced in Section 6.

The average spin magnetic moment of the L-sublattice R_L can be found using the formula:

$$R_L = \sqrt{\left(R^z_L\right)^2 + \left(R^x_L\right)^2}, \quad (37)$$

where the quantities R^z_L and R^x_L are determined by the average occupation numbers of c - and d

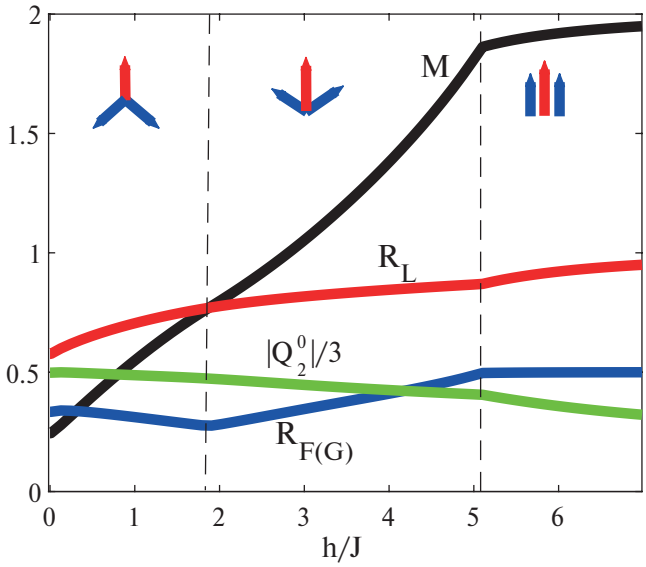

Fig. 5. Dependence of the total moment R_L (red line), $R_{F(G)}$ (blue line), M (black line), and $|Q_2^0|/3$ (green line) on the magnetic field h. The ratio between the exchange integrals is $I/J = 0.8$, while $D/J = 3$. The three pictograms composed of one red and two blue arrows have the same meaning as in Fig. 4.

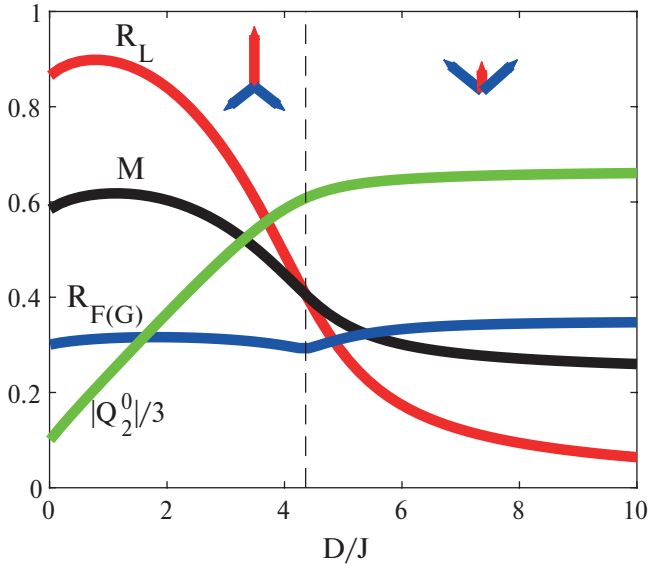

Fig. 6. Dependencies of the quantities R_L (red line), $R_{F(G)}$ (blue line), M (black line), and $|Q_2^0|/3$ (green line) on the anisotropy parameter OA. The ratio between the exchange integrals is $I/J = 0.8$, and $h/J = 1$

-bosons: $n_c = \langle c_k^+ c_k \rangle$ and $n_d = \langle d_k^+ d_k \rangle$, as well as correlators $\langle c_k^+ d_k \rangle$ and $\langle d_k^+ c_k \rangle$. The corresponding expressions are obtained by averaging the formulas given in Appendix C.

Since the total magnetic moment $M = R_F + R_G + R_L$ is directed along the external magnetic field (i.e., along the z-axis), its transverse component must identically vanish:

$$R_L^x + R_F \sin\theta_F + R_G \sin\theta_G = 0,$$

and the longitudinal component equals:

$$M = R_L^z + R_F \cos\theta_F + R_G \cos\theta_G . \qquad (38)$$

The average value of the quadrupole moment [42]:

$$Q_2^0(l) = 3\left(S_l^y\right)^2 - 2 \qquad (39)$$

is calculated similarly after averaging the corresponding formulas from Appendix C.

Fig. 5 shows the dependence of the total moment, the average spin magnetic moments R_L, $R_{F(G)}$, M (black line), and the quadrupole moment $|Q_2^0|/3$ on the magnetic field h for the anisotropy parameter OA $D/J = 3$ and the exchange integral ratio $I/J = 0.8$.

The change in the magnetic field on this figure corresponds to the movement along the horizontal dashed line on the phase diagram in Fig. 4. It is evident that at the transition point from the W phase to the ferromagnetic phase, all curves in Fig. 5 exhibit a kink. The values of M and R_L increase as expected with increasing field h, while the quadrupole moment decreases.

The dependencies of the order parameters M, R_L, R_F, R_G and Q_2^0 on the anisotropy parameter $h/J = 1$ are shown in Fig. 6.

The change in the anisotropy parameter D in this figure corresponds to the movement along the vertical dashed line on the phase diagram in Fig. 4. It can be seen that when crossing the boundary between the $\bar{Y}$ - and W -phases, the dependencies of the order parameters on D exhibit a kink, while the quadrupole moment saturates. The average moment of L-sublattice rapidly decreases near the phase boundary but decreases more slowly with further increase in D.

Clearly, the reduction of R_L facilitates the upward reorientation of the $R_{F(G)}$, vectors, as it reduces the exchange energy loss between the spins $S = 1$ and $S = 1/2$.

An important feature of the phase diagram presented in Fig. 4 is that along the entire boundary between the $\bar{Y}$ - and W -phases (black dashed line), the angle between the vectors R_F and R_G equals π. In this case, from expressions (12) for the effective fields, we find:

$$\bar{H}_z = -h_L, \quad \bar{H}_x = 0. \tag{40}$$

Taking into account these relations and the condition $h_L \neq 0$, the solutions of equations (24) for the angles α_j ($j = 1,2,3$) take the form:

$$2\alpha_1 = \frac{D}{2h_L}(-1)^{n+m}, \quad \alpha_2 = \pi n, \quad \alpha_3 = \pi m, \tag{41}$$

where n and m are integers.

Substituting these solutions into the expressions for the matrix elements of the spin operators from Appendix B gives:

$$s_{11}^z = \cos 2\alpha_1, \quad s_{11}^x = 0. \tag{42}$$

Since $s_{11}^x = 0$ and $\theta_F - \theta_G = \pi$, from equations (25) for the angles θ_F and θ_G, we find the condition:

$$s_{11}^z = h/I_0, \tag{43}$$

which must be satisfied by the matrix element s_{11}^z at the boundary between the $\bar{Y}$- and W-phases. The equation describing the boundary of these phases can be easily obtained from the compatibility condition of the three equations for the angle α_1 and the matrix element s_{11}^z in formulas (41), (42), and (43).

As a result, the following relationship between the model parameters and the magnetic field is obtained:

$$D = \frac{2g_L}{g}\sqrt{I_0^2 - h^2}. \tag{44}$$

This expression analytically describes the dashed line in Fig. 4.

It is important to note that at the points of the phase diagram lying on this dashed line, the orientation of the (antiparallel) vectors R_F and R_G relative to the z-axis is not fixed. This fact implies the degeneracy of the SU3F ground state with respect to the simultaneous rotation of the spins from the F- and G- sublattices around the z-axis, provided that the vectors R_F and R_G remain antiparallel.

Indeed, substituting the solutions (41) for the angles α_j ($j = 1,2,3$) into formulas (22) and (23), as well as fixing the difference in π in exprssion (10) between angles θ_F and θ_G ,, we obtain:

$$\varepsilon_1 = D/2 - \sqrt{h_L^2 + (D/2)^2}, \quad E_0 = -J_0 S^2 N.$$

Thus, at the points of the phase diagram lying strictly on the boundary between the $\bar{Y}$- and W- phases (i.e., along the dashed line in Fig. 4), the ground-state energy $E_{MF} = E_0 + N\varepsilon_1$ (see equation (26)) does not depend on the angles θ_F and θ_G.

The physical reason for this behavior is that, at $\theta_F - \theta_G = \pi$, the two effective fields acting on the spins in the L-sublattice from the F- and G-subsystems compensate each other (see equation (12)). As a result, the L-sublattice effectively "decouples" from both the F- and G-subsystems. Meanwhile, the external magnetic field h_L continues to act on the L-subsystem, aligning the vector R_L along the direction h_L.

Simultaneously, the F- and G-sublattices also "lose connection" with the L-subsystem, as the effective fields generated by it in the F- and G-sublattices are fully canceled by the external magnetic field h. Indeed, as follows from expression (7), the quantities E_a and E_b (see (32)) are precisely the effective fields acting on the spins in the F- and G-sublattices, respectively. Since, at the points lying on the dashed line of the phase diagram in Fig. 4, the conditions (42) and (43) are satisfied, the contributions to effective fields E_a and E_b from the L- subsystem ($-I_0 s_{11}^z \cos\theta_{F(G)}$), the external magnetic field ($h\cos\theta_{F(G)}$) cancel each other out.

Thus, at the points belonging to the dashed line on the phase diagram in Fig. 4, the SU3F system decouples into two effectively non-interacting subsystems: one formed by the S=1 spins of L-sublattice and the other by the $S = 1/2$ spins of F- and G-sublattice spins. In this case, the S=1 spins behave like a paramagnet in an external magnetic field, as they continue to experience the field h_L, while the interaction between them vanishes. The $S = 1/2$ spins behave like a two-sublattice (F and G) collinear antiferromagnet in an effective zero magnetic field. This condition, allowing for an arbitrary orientation of the antiferromagnetic vector in the zx-plane, leads to additional degeneracy of the ground state.

8. PHASE DIAGRAM OF SU3F AT $I/J > 1$

When $I > J$, the phase diagram of SU3F under a magnetic field changes qualitatively. Fig. 7 presents the phase diagram calculated for the exchange parameter ratio $I/J = 1.2$. It is evident that four magnetic phases are realized in this case: the Y-phase, the collinear ferrimagnetic phase, the V ($\bar{V}$) phase, and the ferromagnetic phase.

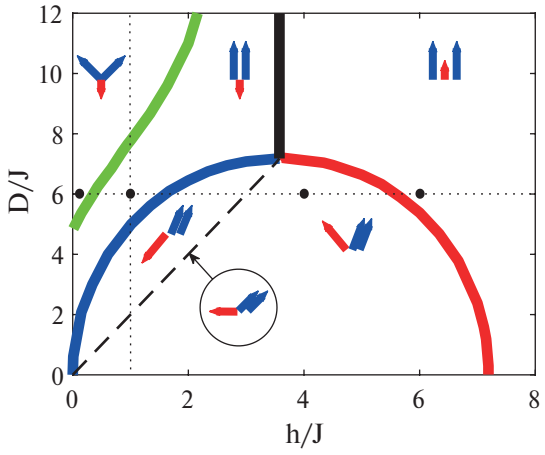

Fig. 7. Phase diagram of the SU3F ground state at $I/J = 1.2$. The green line denotes the boundary between the Y-phase and the collinear ferrimagnetic phase, the blue line separates the collinear ferrimagnetic and $\bar{V}$phases, the black line separates the ferromagnetic and collinear ferrimagnetic phases, the red line separates the ferromagnetic and M phases, and the dashed line marks the boundary between the $\bar{V}$- and V- phases (on this line, $\theta_L = -\pi/2$).

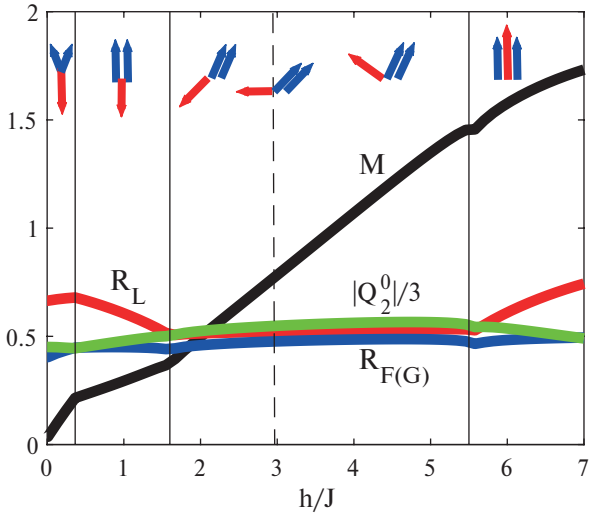

Fig. 8. Dependence of the quantities R_L (red line), $R_{F(G)}$ (blue line), M (black line), and $|Q_2^0|$ (green line) on the external magnetic field h at $I/J = 1.2$ and $D/J = 6$.

In the Y phase, the vector R_L, representing the average spin in the L-sublattice (red arrow in the pictograms of Fig. 7), is directed opposite to the magnetic field (along the $-z$ axis), while the average spin vectors R_F and R_G (blue arrows) in F- and G-sublattices form equal but opposite angles with the z-axis: z: $\theta_F = -\theta_G$, while $|\theta_{F(G)}| \in [0, \pi/2]$.

When transitioning from the Y phase to the collinear ferrimagnetic phase, the angles θ_F and θ_G simultaneously become zero, and all three vectors R_F, R_G and R_L become collinear: the first two align with the magnetic field, while the third opposes it.

Beneath the blue and red curves in Fig. 7 lies the so-called V phase, where the vector R_L forms a nonzero angle θ_L with the z-axis, while the vectors R_F and R_G form equal angles θ_F and θ_G. These angles vary within the range $0, \pi/2$.

This region can be further divided by a dashed line (shown in Fig. 7) into two subregions. To the right of this line, $|\theta_L| < \pi/2$, while to the left, $|\theta_L| > \pi/2$. We retain the V designation for the first region and label the second as the $\bar{V}$ phase for distinction. Along the entire dashed line, the angle θ_L strictly equals $\pi/2$.

In the ferromagnetic phase, all three vectors R_F, R_G and R_L align with the magnetic field.

As in the previous section, to understand the magnetic structure, we examine the changes in order parameters along two directions on the phase diagram: along the horizontal dashed line at a fixed value $D/J = 6$ and along the vertical dashed line at a fixed field $h/J = 1$ (see Fig. 7).

Fig. 8 shows the dependence of the quantities R_L, $R_{F(G)}$, M and Q_2^0 on the external magnetic field h at $D/J = 6$. This corresponds to movement along the horizontal dashed line in Fig. 7.

It is evident that the changes in $R_{F(G)}$ and Q_2^0 with increasing field h are minor, and the reduction in the average spin value $R_{F(G)}$ due to AF interactions is insignificant. In contrast, the average moment of L-sublattice is significantly suppressed due to both AF and OA interactions. In the ferrimagnetic phase, the vector R_L is directed opposite to the field, and its magnitude decreases with increasing h, as expected. In the ferromagnetic phase, the vector R_L aligns with the field, causing its magnitude to increase.

A crucial observation from the graphs in Fig. 8 is that the evolution of the magnetic structure follows the same sequence as in a triangular-lattice antiferromagnet (TLAF) with $S = 1/2$, but without OA [38, 43]. However, while the extended ferrimagnetic (or uud) phase in TLAF can only be explained by quantum fluctuations (which lift accidental degeneracy), in SU3F, this phase arises solely due to OA. Moreover, the behavior of the total moment M qualitatively reproduces the key stages of the TLAF's evolution: the monotonic increase of M in the Y-, $\bar{V}$- and V-phases; a plateau-like region in the ferrimagnetic (uud) phase (commonly referred

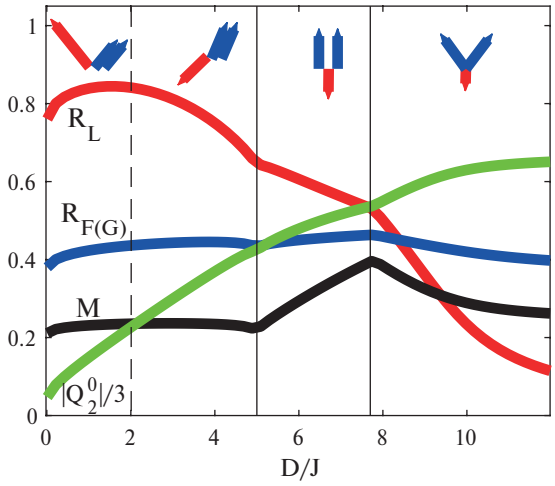

Fig. 9. Dependence of the quantities R_L (red line), $R_{F(G)}$ (blue line), M (black line), and $|Q_2^0|$ (green line) on the parameter D for $I/J = 1.2$ and $D/J = 6$.

to as the 1/3 plateau in TLAF); and the saturation region of M in the ferromagnetic phase, which, however, is less pronounced due to anisotropy.

It is also worth noting that as the anisotropy parameter increases, the existence interval of the $\bar{V}$ and V phases in Fig. 8 shrinks. As follows from the phase diagram in Fig. 7, this interval collapses to a point when $D/J \gtrsim 7$.

Fig. 9 presents the dependence of the quantities R_L, $R_{F(G)}$, M and $|Q_2^0|$ on the anisotropy parameter D at a fixed magnetic field $h/J = 1$. These dependencies correspond to movement along the vertical dashed line in Fig. 7.

It can be seen that the quadrupole moment increases as the anisotropy parameter h increases, while the spin moment R_L from the L-sublattice first slightly increases in the region of low fields and then monotonically decreases. The spin moments $R_{F(G)}$ from the F- and G-sublattices do not significantly change throughout the entire range of D. Therefore, the noticeable increase in the total moment M in the ferromagnetic phase is not due to changes in the orientation or absolute values of $R_{F(G)}$, but rather due to the decrease in R_L caused by the anisotropy. Upon transition to the Y-phase, the total moment M begins to decrease, as the rotation of the vectors R_F and R_G around the y-axis reduces their projection onto the z-axis.

The three vertical lines in Fig. 9 divide the four previously described phases. During the transitions from the V-phase to the ferromagnetic phase and from the ferromagnetic phase to the Y-phase, all order parameter dependencies exhibit a kink. At the same time, the transition from the V-phase to the $\bar{V}$-phase is not accompanied by any anomalies in the presented dependencies.

9. GROUND-STATE DEGENERACY AT $I = J$

The case $I = J$ is special because the classical analog of the SU3F Hamiltonian, as we will now show, exhibits continuous accidental degeneracy.

Indeed, let us define the Hamiltonian dependent on the parameter λ:

$$H_\lambda = J\sum_{\{fg\}} S_f S_g + \lambda J\sum_{\{fl\}} S_f S_l + \lambda J\sum_{\{gl\}} S_g S_l + \\ + D\sum_l \left(S_l^y\right)^2 - h\left(\sum_f S_f + \sum_g S_g + \lambda\sum_l S_l\right), \quad (45)$$

where the direction of the magnetic field $h = g\propto_B H$ is generally arbitrary. All the notations in Equation (45) are the same as in the Hamiltonian (1). It is evident that if the conditions $\lambda = I/J = g_L/g$ are met for λ and the field h is directed along the z-axis, the Hamiltonian (45) coincides with the operator H defined by Equation (1).

On the other hand, it is easy to verify that the Hamiltonian (45), up to the constant

$$-JN\left(\frac{3}{2}\lambda^2 S_L(S_L+1) + \frac{9}{4} + \frac{h^2}{6J^2}\right), \quad S_L = 1, \quad (46)$$

can be represented as

$$H_\lambda = D\sum_l \left(S_l^y\right)^2 + \\ + \frac{J}{4}\sum_p \left(S_{pF} + S_{pG} + \lambda S_{pL} - \frac{h}{3J}\right)^2, \quad (47)$$

where the sum p runs over all triangular plaquettes, and the lower indices F, G and L of the spin operators indicate their belonging to the corresponding sublattices in the p-th plaquette.

Thus, if the SU3F parameters satisfy the condition

$$\frac{I}{J} = \frac{g_L}{g}, \quad (48)$$

then the SU3F Hamiltonian in Equation (1) can be represented in the form of Equation (47) with the field h directed along the z-axis.

If we now consider classical moments instead of spin operators in Equation (47), i.e., ordinary vectors of fixed length, it is easy to see that the minimum value of the Hamiltonian (47) will be achieved when both of its terms vanish. The vanishing of the first term implies that the spins of the L-sublattice lie in the easy-plane zx. The requirement for the second term in (47) to vanish reduces to the equation

$$S_{pF} + S_{pG} + \lambda S_{pL} - \frac{h}{3J} = 0. \qquad (49)$$

It is evident that, for certain values of the magnetic fields h, this equation can be satisfied by an infinite set of solutions, i.e., different orientations of the three vectors R_L, R_F and R_G, even when the field h does not lie in the zx-plane. Moreover, if the magnetic field is parallel to the zx-plane (as in our case), the orientation of the vectors R_L, R_F and R_G, which minimizes the Hamiltonian (47), may not necessarily be coplanar with the zx-plane.

The above analysis of the classical limit of the Hamiltonian (47) suggests that the observed (continuous) degeneracy of the SU3F ground state should also hold in the quantum case when the condition (48) is satisfied. Our calculations using the mean-field approximation at $I = J$ and $g_L = g$ confirmed that this is indeed the case.

Similar degeneracy occurs in other quantum magnets, such as the antiferromagnet on a triangular lattice (AFTL) with $S = 1/2$ [43]. As was first demonstrated in [38], this degeneracy can be lifted by considering zero-point quantum fluctuations. This approach requires taking into account higher-order terms (compared to the harmonic approximation used in this work) when bosonizing spin operators within the Holstein–Primakoff representation for the F- and G-subsystems and within the indefinite metric formalism for the L-subsystem.

For this reason, constructing the phase diagram of SU3F at critical parameters satisfying the condition (48) will be carried out by the authors in a separate study.

10. SPIN-WAVE EXCITATIONS IN SU3F UNDER A MAGNETIC FIELD

The spectral properties of SU3F in the absence of a magnetic field were thoroughly studied in [31]. In this section, we analyze changes in the spectrum under a nonzero magnetic field while keeping the anisotropy parameter OA fixed. Four dispersion curves ε_{jk} $(j = 1,\ldots,4)$ were calculated for each set of model parameters based on equation (33) derived in Section 6.

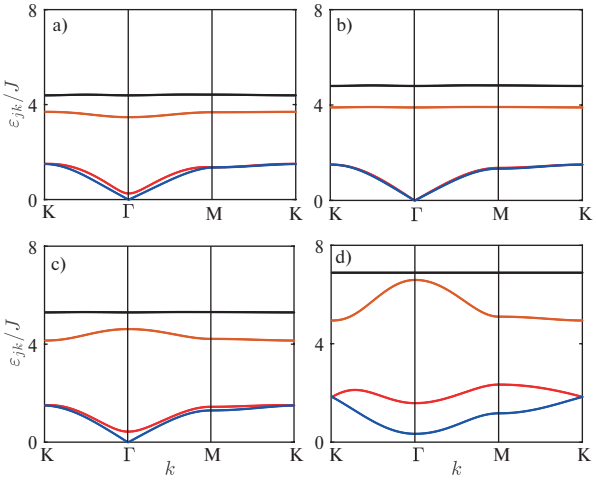

Fig. 10. Spin-wave excitation spectra at $I/J = 0.8$, $D/J = 3$, and four external magnetic field strengths: $h/J = 1$ (*a*), 1.87 (*b*), 3 (*c*), 5.5 (*d*). The wave vector k traverses the triangular path ΓKM in the Brillouin zone (see Fig. 3).

Fig. 10 shows the results of numerical calculations of the dispersion curves for four different magnetic field strengths with the model parameters $I/J = 0.8$ and $D/J = 3$. On the phase diagram in Fig. 4, the four black dots along the horizontal dashed line correspond to these four field values. It is evident that at $h/J = 1$, the system is in the $\bar{Y}$ phase; at $h/J = 1.87$, the system is in the antiparallel phase for the F- and G-sublattices; at $h/J = 3$ the system transitions into the W phase; and at $h/J = 5.5$, the system reaches the ferromagnetic phase. Each of the four panels in Fig. 10 displays four dispersion curves corresponding to the four types of introduced bosons. However, only one curve (black in all graphs) can be confidently associated with the high-energy d-bosons. The other three branches are formed through the hybridization of the a-, b- and c-boson states.

Crucial observation is that in the first three graphs (a, b, c), there is at least one Goldstone mode (blue curves) associated with the breaking of symmetry in the ground state due to the collective rotation of spins in the F- and G-sublattices around the magnetic field direction. In the ferromagnetic phase (Fig. 10d), the ground state does not break this symmetry, and thus, the Goldstone (gapless) mode is absent.

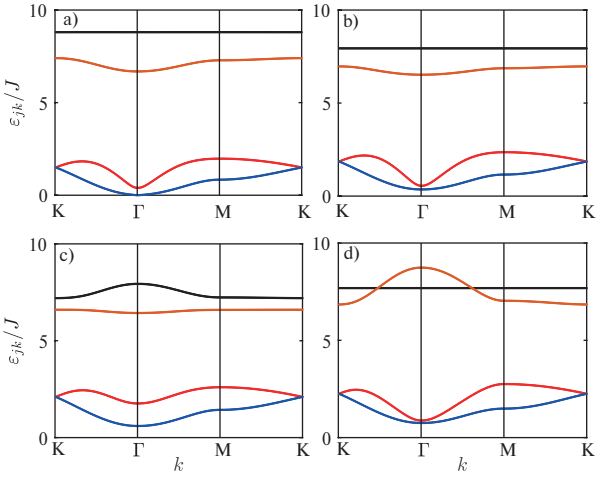

Fig. 11. Spin-wave excitation spectra at $I/J = 1.2$, $D/J = 6$ and four external magnetic field strengths: $h/J = 0.3$ (*a*), 1 (*b*), 4 (*c*), 6 (*d*). The wave vector k traverses the triangular path ΓKM in the Brillouin zone (see Fig. 3).

In Fig. 10b, two Goldstone modes appear (coincident blue and red curves). The origin of the second mode relates to the phase diagram feature discussed in Section 7, specifically the dashed curve (see Fig. 4). In this scenario, the moments R_F and R_G align along the zx -plane in opposite directions, causing the system's energy to degenerate with respect to the rotation of the R_F and R_G vector line around the y-axis.

As mentioned in Section 7, this behavior is due to the vanishing of effective fields and the effective decoupling of the L-subsystem from the F- and G-subsystems. In such a case, the nodes of the L-sublattice become effectively isolated (even from each other), which explains the flat dispersion of the two high-energy branches (black and brown) in Fig. 10b.

The dispersion dependencies ε_{jk} shown in Fig. 11 were calculated with the following model parameters: $I/J = 1.2$, $D/J = 6$, for four values of the external magnetic field: $h/J = 0.3$, 1, 4 and 6. On the phase diagram in Fig. 7, these four field values correspond to the four black dots along the horizontal dashed line. As the magnetic field h increases, the system sequentially transitions through the following four phases: the $\bar{Y}$ phase at $h/J = 0.3$; the ferrimagnetic phase at $h/J = 1$; the V- phase at $h/J = 4.3$; and the ferromagnetic phase at $h/J = 6$.

From the graphs presented in Fig. 11, it is evident that the Goldstone mode appears only in the first case (Fig. 10a), as the breaking of ground-state symmetry (relative to rotations around the z-axis) occurs exclusively in the $\bar{Y}$-phase. In all other regions of the phase diagram (Fig. 7), the spin-wave excitation spectrum remains gapped.

11. CONCLUSION

The main outcome of this study is the construction of the phase diagram of the SU3F ferrimagnet on a triangular lattice, plotted in the coordinates of the magnetic field h (applied in the easy-plane anisotropy plane) and the single-ion anisotropy parameter D at zero temperature. Among the key features of the SU3F model, the following three stand out: 1) different spin magnitudes in magnetic sublattices: two sublattices (F and G) have spin $S = 1/2$, while the third L-sublattice has spin $S = 1$; 2) single-ion anisotropy: easy-plane anisotropy acts on the L-sublattice with spin S=1; 3) different exchange integrals: The exchange interactions differ between the F- and G-sublattices (J) and between the L- F(G) sublattices (I).

Numerical calculations under the mean-field approximation revealed two qualitatively distinct types of SU3F phase diagrams depending on the ratio between the exchange integrals I and J. These phase diagrams differ both in the number of realized phases and in the nature of their magnetic structures.

For $I < J$, the ground state of SU3F can be characterized by three magnetic configurations: the $\bar{Y}$, W phase, and the ferromagnetic phase (see Fig. 4). Notably, along the boundary between the $\bar{Y}$ - and W -phases (dashed line in Fig. 4), the SU3F system effectively splits into two independent magnetic subsystems/ The first subsystem consists of spin-1 sites on a triangular lattice and behaves as a paramagnet. Another one consists of $S = 1/2$ spins forming a planar hexagonal lattice in a collinear two-sublattice antiferromagnetic phase under an effective zero magnetic field. This decoupling leads to an additional degeneracy of the ground state, associated with the free rotation of the antiferromagnetic vector within the easy-plane. This degeneracy manifests as an extra Goldstone mode in the spin-wave excitation spectrum.

For the reverse exchange ratio ($I > J$), the SU3F the h–D- phase diagram undergoes significant changes. It now features four distinct regions characterized by different magnetic ground-state structures, i.e. the Y- phase, two collinear ferrimagnetic and ferromagnetic phases, as well as the V-phase. The V-phase can further be subdivided into two sub-phases ($\bar{V}$ and V), depending on whether the angle θ_L exceeds the critical value $\pi/2$.

For both $I < J$ and $I > J$, the quadrupole and dipole order parameters were analyzed as functions of both the magnetic field (at fixed anisotropy OA) and the anisotropy parameter OA (at fixed magnetic field h). One significant result of this study is the dependence of the total moment M on the external magnetic field. For $I > J$ and a specific finite value of OA, this dependence qualitatively reproduces the well-known behavior observed in quantum antiferromagnets on a triangular lattice with uniform spin $S = 1/2$ and without anisotropy [38, 43]. Specifically, within a certain magnetic field range, the magnetization curve exhibits a plateau (albeit with a slight tilt in our case). In conventional quantum triangular-lattice antiferromagnets (QTAFMs), this plateau arises due to quantum antiferromagnetic fluctuations, while in SU3F, it emerges due to the presence of single-ion anisotropy.

A notable finding is the qualitative difference between the two phase diagrams for $I < J$ and $I > J$. There is no continuous transformation at $I \to J$ from one diagram to the other. This is because, when the exchange integrals become equal ($I = J$), accidental degeneracy arises, leading to an ambiguity in the magnetic configuration within the mean-field approximation for given magnetic field and anisotropy values. We hypothesize that, as with QTAFMs, quantum fluctuations should lift the observed accidental degeneracy (as well as the additional degeneracy noted for $I < J$). However, a detailed investigation of this issue requires further study and will be addressed in future research.

In conclusion, we emphasize that in the present study, the magnetic field h applied to the quantum SU3F system was oriented within the easy-plane anisotropy plane. If the magnetic field were instead applied perpendicular to this plane, the behavior of the magnetic order parameters could differ qualitatively.

ACKNOWLEDGMENTS

The authors express their gratitude to Professor V.V. Valkov for his assistance in formulating the research problem, providing valuable advice, and stimulating discussions regarding the obtained results.

FUNDING

This study was conducted within the framework of the scientific program of the State Assignment of the Institute of Physics of the Siberian Branch of the Russian Academy of Sciences (IF SB RAS).

APPENDIX A. UNITARY TRANSFORMATION OF HUBBARD OPERATORS

As a result of the unitary transformations of the Hubbard operators according to formula (20), with the unitary operator $U_{\tilde{n}\tilde{m}}(\alpha)$ ($n \neq m$)defined by formula (20), the following expressions are obtained [40]:

$$\begin{aligned}
X^{nn} &= \cos^2\alpha X^{\tilde{n}\tilde{n}} + \sin^2\alpha X^{\tilde{m}\tilde{m}} - \\
&-\frac{1}{2}\sin 2\alpha\left(X^{\tilde{n}\tilde{m}} + X^{\tilde{m}\tilde{n}}\right), \\
X^{mm} &= \cos^2\alpha X^{\tilde{m}\tilde{m}} + \sin^2\alpha X^{\tilde{n}\tilde{n}} + \\
&+\frac{1}{2}\sin 2\alpha\left(X^{\tilde{n}\tilde{m}} + X^{\tilde{m}\tilde{n}}\right), \\
X^{nm} &= \cos^2\alpha X^{\tilde{n}\tilde{m}} - \sin^2\alpha X^{\tilde{m}\tilde{n}} + \\
&+\frac{1}{2}\sin 2\alpha\left(X^{\tilde{n}\tilde{n}} - X^{\tilde{m}\tilde{m}}\right), \\
X^{mn} &= \cos^2\alpha X^{\tilde{m}\tilde{n}} - \sin^2\alpha X^{\tilde{n}\tilde{m}} + \\
&+\frac{1}{2}\sin 2\alpha\left(X^{\tilde{n}\tilde{n}} - X^{\tilde{m}\tilde{m}}\right), \\
X^{np} &= \cos\alpha X^{\tilde{n}\tilde{p}} - \sin\alpha X^{\tilde{m}\tilde{p}}, \\
X^{pn} &= \cos\alpha X^{\tilde{p}\tilde{n}} - \sin\alpha X^{\tilde{p}\tilde{m}}, \\
X^{pm} &= \cos\alpha X^{\tilde{p}\tilde{m}} + \sin\alpha X^{\tilde{p}\tilde{n}}, \\
X^{mp} &= \cos\alpha X^{\tilde{m}\tilde{p}} + \sin\alpha X^{\tilde{n}\tilde{p}}, \\
X^{pq} &= X^{\tilde{p}\tilde{q}},
\end{aligned}$$

where all four state indices p, q, n and m are different, and the site indices are omitted. In the main text, for brevity, the tilde notation, indicating the new (transformed) states, is not used for the indices of the thrice-transformed Hubbard operators.

APPENDIX B. MATRIX ELEMENTS OF SPIN OPERATORS

This appendix presents the explicit form of the matrix elements $s^{\alpha}_{nm} \equiv \langle n \mid S^{\alpha}_{l} \mid m \rangle$ ($\alpha = \{x,y,z\}$ and $n,m = \{\bar{1},0,1\}$),, used in the decomposition (27). These elements were obtained from the three successive transformations of the Hubbard operators using the three unitary operators $U_{1-1}(-\alpha_1)$, $U_{0-1}(-\alpha_3)$ and $U_{10}(-\alpha_2)$, followed by substituting

the transformed results into the representation (15) for the spin operators of the L -sublattice.

Matrix elements for the spin operator S_l^z :

$$s_{11}^z = (\cos\alpha_1\cos\alpha_2 + \sin\alpha_1\sin\alpha_2\sin\alpha_3)^2 -$$

$$-\sin^2\alpha_1\cos^2\alpha_3,$$

$$s_{\bar{1}\bar{1}}^z = (\cos\alpha_1\sin\alpha_2\sin\alpha_3 - \sin\alpha_1\cos\alpha_2)^2 -$$

$$-\cos^2\alpha_1\cos^2\alpha_3,$$

$$s_{00}^z = \sin^2\alpha_2\cos^2\alpha_3 - \sin^2\alpha_3,$$

$$s_{10}^z = s_{01}^z = -\frac{1}{2}\sin\alpha_1(1+\sin^2\alpha_2)\sin 2\alpha_3 -$$

$$-\frac{1}{2}\cos\alpha_1\sin(2\alpha_2)\cos\alpha_3,$$

$$s_{1\bar{0}}^z = s_{0\bar{1}}^z = -\frac{1}{2}\cos\alpha_1(1+\sin^2\alpha_2)\sin 2\alpha_3 +$$

$$+\frac{1}{2}\sin\alpha_1\sin(2\alpha_2)\cos\alpha_3,$$

$$s_{\bar{1}1}^z = s_{1\bar{1}}^z = \frac{1}{2}\cos 2\alpha_1\sin 2\alpha_2\sin\alpha_3 +$$

$$+\frac{1}{2}\sin 2\alpha_1(\sin^2\alpha_2\sin^2\alpha_3 - \cos^2\alpha_3 - \cos^2\alpha_2).$$

For the operator S_l^x :

$$s_{11}^x = \sqrt{2}(\cos\alpha_1\sin\alpha_2 -$$

$$-\sin\alpha_1\sin\alpha_3\cos\alpha_2)(\cos\alpha_1\cos\alpha_2 +$$

$$+\sin\alpha_1\sin\alpha_3\sin\alpha_2 + \sin\alpha_1\cos\alpha_3),$$

$$s_{\bar{1}\bar{1}}^x = \sqrt{2}(\sin\alpha_1\sin\alpha_2 +$$

$$+\cos\alpha_1\sin\alpha_3\cos\alpha_2)(\sin\alpha_1\cos\alpha_2 -$$

$$-\cos\alpha_1\sin\alpha_3\sin\alpha_2 - \cos\alpha_1\cos\alpha_3),$$

$$s_{00}^x = \frac{1}{\sqrt{2}}(\cos\alpha_2\sin 2\alpha_3 - \sin 2\alpha_2\cos^2\alpha_3),$$

$$s_{\bar{1}1}^x = \frac{\cos 2\alpha_1}{\sqrt{2}}(\sin\alpha_2\cos\alpha_3 - \sin\alpha_3\cos 2\alpha_2) -$$

$$-\frac{\sin 2\alpha_1}{2\sqrt{2}}(\cos\alpha_2\sin 2\alpha_3 + \sin 2\alpha_2(1+\sin^2\alpha_3)),$$

$$s_{10}^x = \frac{\cos\alpha_1}{\sqrt{2}}(\cos 2\alpha_2\cos\alpha_3 + \sin\alpha_2\sin\alpha_3) +$$

$$+\frac{\sin\alpha_1}{\sqrt{2}}(\cos\alpha_2\cos 2\alpha_3 + \frac{1}{2}\sin 2\alpha_2\sin 2\alpha_3),$$

$$s_{\bar{1}0}^x = -\frac{\sin\alpha_1}{\sqrt{2}}(\cos 2\alpha_2\cos\alpha_3 + \sin\alpha_2\sin\alpha_3) +$$

$$+\frac{\cos\alpha_1}{\sqrt{2}}(\cos\alpha_2\cos 2\alpha_3 + \frac{1}{2}\sin 2\alpha_2\sin 2\alpha_3),$$

$$s_{\bar{1}1}^x = s_{1\bar{1}}^x, \quad s_{10}^x = s_{01}^x, \quad s_{\bar{1}0}^x = s_{0\bar{1}}^x.$$

For the operator S_l^y :

$$s_{11}^y = s_{\bar{1}\bar{1}}^y = s_{00}^y = 0,$$

$$s_{01}^y = \frac{i}{\sqrt{2}}(-\sin\alpha_1\cos\alpha_2 +$$

$$+\cos\alpha_1(\cos\alpha_3 + \sin\alpha_2\sin\alpha_3)),$$

$$s_{\bar{1}0}^y = \frac{i}{\sqrt{2}}(\cos\alpha_1\cos\alpha_2 +$$

$$+\sin\alpha_1(\cos\alpha_3 + \sin\alpha_2\sin\alpha_3)),$$

$$s_{\bar{1}1}^y = \frac{i}{\sqrt{2}}(\sin\alpha_2\cos\alpha_3 - \sin\alpha_3),$$

$$s_{\bar{1}1}^y = -s_{1\bar{1}}^y, \quad s_{10}^y = -s_{01}^y, \quad s_{\bar{1}0}^y = -s_{0\bar{1}}^y.$$

For the operator $(S_l^y)^2$:

$$\langle 1 \mid (S_l^y)^2 \mid 1\rangle = \frac{1}{2} + \frac{1}{2}\cos^2\alpha_1\sin^2\alpha_2 +$$

$$+\frac{1}{2}\sin^2\alpha_1(\cos^2\alpha_2\sin^2\alpha_3 - \sin\alpha_2\sin 2\alpha_3) -$$

$$-\frac{1}{2}\sin 2\alpha_1\cos\alpha_2(\sin\alpha_2\sin\alpha_3 + \cos\alpha_3),$$

$$\langle \bar{1} \mid (S_l^y)^2 \mid \bar{1}\rangle = \frac{1}{2} + \frac{1}{2}\sin^2\alpha_1\sin^2\alpha_2 +$$

$$+\frac{1}{2}\cos^2\alpha_1(\cos^2\alpha_2\sin^2\alpha_3 - \sin\alpha_2\sin 2\alpha_3) +$$

$$+\frac{1}{2}\sin 2\alpha_1\cos\alpha_2(\sin\alpha_2\sin\alpha_3 + \cos\alpha_3),$$

$$\langle 0 \mid (S_l^y)^2 \mid 0\rangle = \frac{1}{2}(\sin\alpha_2\sin 2\alpha_3 +$$

$$+1 + \cos^2\alpha_2\cos^2\alpha_3),$$

$$\langle \bar{1} \mid (S_l^y)^2 \mid 1\rangle = \frac{1}{4}(\cos^2\alpha_2\sin^2\alpha_3 -$$

$$-\sin\alpha_2\sin 2\alpha_3 - \sin^2\alpha_2)\sin 2\alpha_1 -$$

$$-\frac{1}{2}\cos 2\alpha_1\cos\alpha_2(\sin\alpha_2\sin\alpha_3 + \cos\alpha_3),$$

$$\langle \bar{1} \mid (S_l^y)^2 \mid 0\rangle = \frac{1}{2}\sin\alpha_1\cos\alpha_2(\sin\alpha_3 - \sin\alpha_2\cos\alpha_3) +$$

$$+\frac{1}{2}\cos\alpha_1\left(\sin\alpha_2\cos 2\alpha_3 - \frac{1}{2}\cos^2\alpha_2\sin(2\alpha_3)\right),$$

$$\langle 1 \mid (S_l^y)^2 \mid 0\rangle = \frac{1}{2}\cos\alpha_1\cos\alpha_2(\sin\alpha_2\cos\alpha_3 - \sin\alpha_3) +$$

$$+\frac{1}{2}\sin\alpha_1\left(\sin\alpha_2\cos 2\alpha_3-\frac{1}{2}\cos^2\alpha_2\sin(2\alpha_3)\right),$$

$$\langle 1|(S_l^y)^2|\bar{1}\rangle=\langle\bar{1}|(S_l^y)^2|1\rangle,\quad \langle 0|(S_l^y)^2|\bar{1}\rangle=\langle\bar{1}|(S_l^y)^2|0\rangle,$$

$$\langle 0\mid(S_l^y)^2\mid 1\rangle=\langle 1\mid(S_l^y)^2\mid 0\rangle.$$

APPENDIX C. BOSONIZATION OF SPIN OPERATORS FOR S=1

Using the representation (28) in formulas (27) and retaining only terms up to the second order in boson operators, the following spin operator expressions through bosonic operators are obtained:

$$S_l^x=\frac{1}{\sqrt{2}}[(s_{0,1}^x(c_l^+ + c_l)+s_{\bar{1},1}^x(d_l^+ + d_l)+$$

$$+s_{\bar{1},0}^x(d_l^+c_l + c_l^+d_l)+s_{\bar{1},1}^x+(s_{0,0}^x - s_{1,1}^x)c_l^+c_l +$$

$$+(s_{\bar{1},\bar{1}}^x - s_{1,1}^x)d_l^+d_l],$$

$$S_l^y=\frac{i}{\sqrt{2}}[s_{0,1}^y(c_l^+ - c_l)+s_{\bar{1},1}^y(d_l^+ - d_l)+$$

$$+s_{\bar{1},0}^y(d_l^+c_l - c_l^+d_l)],$$

$$S_l^z=s_{0,1}^z(c_l^+ + c_l)+s_{\bar{1},1}^z(d_l^+ + d_l)+$$

$$+s_{\bar{1},0}^z(d_l^+c_l + c_l^+d_l)+s_{\bar{1},1}^z+(s_{0,0}^z - s_{1,1}^z)c_l^+c_l +$$

$$+(s_{\bar{1},\bar{1}}^z - s_{1,1}^z)d_l^+d_l,$$

$$(S_l^y)^2=\frac{1}{2}[((s_{\bar{1},0}^y)^2-(s_{\bar{1},1}^y)^2)c_l^+c_l +$$

$$+((s_{\bar{1},0}^y)^2-(s_{0,1}^y)^2)d_l^+d_l -$$

$$-s_{\bar{1},0}^y s_{0,1}^y(d_l^+ + d_l)+s_{\bar{1},0}^y s_{\bar{1},1}^y(c_l^+ + c_l)+$$

$$+((s_{0,1}^y)^2+(s_{\bar{1},1}^y)^2)+s_{0,1}^y s_{\bar{1},1}^y(d_l^+c_l + c_l^+d_l)].$$

The presented expressions, after averaging and applying the spectral theorem to compute the boson operator expectations, were used to derive the formulas for calculating the order parameters R_L, M and Q_2^0.

REFERENCES

1. *B. Barbara, Y. Imry, G. Sawatzky, and P. C. E. Stamp*, Quantum Magnetism NATO: Science for Peace and Security, Series B: Physics and Biophysics, Springer Dordrecht (2008).
2. *Introduction to Frustrated Magnetism*, Springer Series in Solid-State Sciences, ed. by C. Lacroix, P. Mendels, and F. Mila (2011).
3. *A. Auerbach*, Interacting Electrons and Quantum Magnetism, Springer-Verlag, New York, Inc. (1994).
4. *V. V. Val'kov, S. G. Ovchinnikov*, Theoretical and Mathematical Physics, **50**, 306 (1982).
5. *H. H. Chen and P. M. Levy*, Phys. Rev. Lett. **27**, 1383 (1971).
6. *V. M. Matveev*, JETP **38**, 813 (1973).
7. *M. P. Kashchenko, N. F. Balakhonov, and L. V. Kurbatov*, JETP **37**, 201 (1973).
8. *V. M. Loktev and V. S. Ostrovskii*, Ukr. J. Phys. **23**, 1717 (1978).
9. *F. P. Onufrieva*, JETP **53**, 1241 (1981).
10. *A. F. Andreev and I. A. Grishchuk*, JETP **60**, 267 (1984).
11. *F. P. Onufrieva*, JETP **62**, 1311 (1985).
12. *N. Papanicolaou*, Nucl. Phys. B **305**, 367 (1988).
13. *A. V. Chubukov*, J. Phys.: Condens. Matter **2**, 1593 (1990).
14. *V. V. Val'kov and T. A. Val'kova*, JETP **72**, 1053 (1991).
15. *Yu. A. Fridman, O. A. Kosmachev, and Ph. N. Klevets*, J. Magn. Magn. Mat. **325**, 125 (2013).
16. A. I. Smirnov, Physics Uspekhi 59, 564 (2016)].
17. *O. A. Kosmachev, Ya. Yu. Matyunina, and Yu. A. Fridman*, JETP **135**, 354 (2022).
18. *H. F. Verona de Resende, F. C. SaBarreto, and J. A. Plascak*, Physica A **149**, 606 (1988).
19. *G. M. Zhang and C. Z. Yang*, Phys. Rev. B **48**, 9452 (1993).
20. *A. Bobak and M. Jurcisin*, Physica A *240*, 647 (1997)
21. *G. M. Buendia and M. A. Novotny*, J. Phys.: Condens. Matter **9**, 5951 (1997).
22. *M. Godoy and W. Figueiredo*, Physica A **339**, 392 (2004).
23. *T. Iwashita and N. Uryu*, J. Phys. Soc. Japan **53**, 721 (1984).
24. *J. Oitmaa*, Phys. Rev. B **72**, 224404 (2005).
25. *J. Oitmaa and I. G. Enting*, J. Phys.: Condens. Matter **18**, 10931 (2006).
26. *W. Selke and J. Oitmaa*, J. Phys.: Condens. Matter **22**, 076004 (2010).
27. *Yu. A. Fridman and O. A. Kosmachev*, Physics of the Solid State **51**, 1167 (2009).
28. *M. Zukovic and A. Bobak*, Phys. Rev. E **91**, 052138 (2015).
29. *M. Zukovic and A. Bobak*, Physica A **436** 509 (2015).
30. *E. S. de Santana, A. S. de Arruda, and M. Godoy*, Condensed Matter Physics, **26**, 23601 (2023)
31. *A. S. Martynov and D. M. Dzebisashvili*, J. Magn. Magn. Mat. **584**, 171906 (2024).

32. *B. A. Ivanov and A. K. Kolezhuk*, Phys. Rev. B **68**, 052401 (2003).

33. *A. Lauchli, F. Mila, and K. Penc*, Phys. Rev. Lett. **97**, 087205 (2006).

34. *V. V. Val'kov and M. S. Shustin*, JETP **121**, 860 (2015)].

35. *V. V. Val'kov and M. S. Shustin*, J. Low Temp. Phys. **185**, 564 (2016).

36. *Yu. A. Fridman and D. V. Spirin*, J. Magn. Magn. Mat. **253**, 111 (2002).

37. *J. Hubbard*, Proc. Roy. Soc. A **281**, 401 (1964).

38. *A. V. Chubukov and D. I. Golosov*, J. Phys.: Condens. Matter ***3***, 69 (1991).

39. *C. Cohen-Tannoudji, B. Diu, and F. Laloe*, Wiley-VCH (2019), Vol. 1.

40. *V. V. Val'kov*, Theor. Math. Phys. **76**, 766 (1988).

41. *A. I. Akhiezer, V. G. Bar'yakhtar, and S. V. Peletminskii*, Spin Waves, Published by North-Holland Publishing Company, Amsterdam, 1968.

42. *L. D. Landau and E. M. Lifshitz*, Quantum Mechanics: Non-Relativistic Theory, Elsevier (2013), Vol. 3.

43. *T. Coletta, T. A. Toth, K. Penc at al.*, Phys. Rev. B **94**, 075136 (2016).